*Article*

# An Inverted Perovskite Solar Cell with Good Comprehensive Performance Realized by Reducing the Concentration of Precursors

Lijia Chen [1,*,†], Cunyun Xu [2,†], Yan Qin [3], Xiaofeng He [2], Hongyu Bian [2], Gaobo Xu [2], Lianbin Niu [1] and Qunliang Song [2,*]

1   College of Physics and Electronic Engineering, Chongqing Normal University, Chongqing 401331, China; niulb03@126.com
2   Institute for Clean Energy and Advanced Materials, School of Materials and Energy, Southwest University, Chongqing 400715, China; cyxuamos@foxmail.com (C.X.); hexf1992@163.com (X.H.); samuelhbian@163.com (H.B.); gbxu1805@163.com (G.X.)
3   Foundation Department, Army Logistics Academy, Chongqing 401331, China; qy.yfds@foxmail.com
*   Correspondence: ljchen01@cqnu.edu.cn (L.C.); qlsong@swu.edu.cn (Q.S.)
†   These authors contributed equally to this work.

**Abstract:** Inverted perovskite solar cells (PSCs) exhibit great potential for industrial application thanks to their low complexity and low fabrication temperature. Aiming at commercial applications, it is necessary to comprehensively consider the material consumption and its corresponding electrical performance. Here, a simple strategy has been proposed to obtain inverted PSCs with comprehensive performance, that is, reaching an acceptable electrical performance by reducing the usage of perovskite. More precisely, the inverted PSCs, whose perovskite film is prepared by 1.0 M precursor, yields a power conversion efficiency (*PCE*) of 15.50%, fulfilling the requirement for real commercial application. In addition, the thickness of the electron transport layer ($C_{60}$ in this work) in the above inverted PSCs was further optimized by comparing the simulated absorption spectrum, *J-V* characteristics and impedance with three different thicknesses of $C_{60}$ layer. More excitingly, the optimized device displays high storage stability which maintains more than 90% of its initial *PCE* for 28 days. Therefore, our work provides a simple and cost-effective method to reach good comprehensive performance of inverted PSCs for commercial applications.

**Keywords:** inverted PSCs; comprehensive performance; material consumption; commercial application

## 1. Introduction

Organic-inorganic hybrid perovskite materials, combining the facile processing of organic semiconductors with the high charge carrier transport property of inorganic materials, are one of the most promising candidates for the next generation of solar cells [1–4]. During the last decade, we have witnessed a dramatic increase in the power conversion efficiency (*PCE*) of perovskite solar cells (PSCs) from 3.8% to 25.7%, which is comparable to or even exceeds silicon-based solar cells [5,6]. It is worth pointing out that most of the highly efficient PSCs are achieved in regular (*n-i-p*) structures [7,8], in which *n* and *p* represent the electron transport layer (ETL) and hole transport layer (HTL), respectively [9,10]. As compared to regular devices, inverted PSCs (*p-i-n*) always exhibit a bit lower *PCE* but high opportunity for industrial application thanks to their relatively simple structure, with less energy consumption during fabrication and negligible hysteresis of device performance [11–13]. Therefore, much effort has been devoted to enhancing the *PCE* of inverted PSCs. For instance, thickness optimizations and electrical/optical characterizations have been employed in PSCs. Du et al. reported fabrication of relatively thick perovskite layers can considerably improve the average *PCE* under normal operational conditions [14]. Santos et al. reported optimizing film thicknesses in the search of major

efficiency improvements, and the thickness of 400 nm for perovskite layer showed a benefit of significant absorption of light and reducing defects, which is facilitated by increasing quantum efficiency [15]. Koç et al. reported thickness optimizations of transport layers, perovskite and transparent conductive oxides to improve antireflection and light trapping properties, and to therefore maximize the photocurrent of PSCs [16]. Xu et al. reported high *PCE* inverted PSCs (reached 19.49%) based on MAPbI$_3$(Cl) by employing self-woven deposited poly(3,4-ethylenedioxythiophene):polystyrenesulfonate(PEDOT:PSS) as HTL [11]. At the same time, Li et al. reported an inverted PSC based on a (FAPbI$_3$)$_{0.95}$(MAPbBr$_3$)$_{0.05}$ active layer with the highest *PCE* so far (>24%) by utilizing surface sulfidation treatment on the perovskite film [7].

Aside from the continuous enhancement of electrical performance in inverted PSCs, comprehensive consideration of material consumption and electrical device performance is another primary factor for their future development, especially for their commercial application. Unfortunately, there have been less reports on this issue. To lower material consumption, reducing the use of perovskite is likely the first method that comes to mind. However, the reduction of perovskite usage (e.g., reducing perovskite precursor concentration) directly leads to a decrease in the thickness of perovskite film, which is detrimental to light absorption and then inevitably decreases the *PCE* of the device [16,17]. Nevertheless, an appropriate reduction of *PCE* is acceptable if we consider that solar cells can reach a viable level for commercialization once their efficiency reaches ~15% [18]. Within this context, it is necessary to reach a balance between electrical performance and material consumption.

In this work, by tuning the concentration of perovskite precursor and comparing their corresponding electrical performance, a balance between material consumption and electrical performance has been achieved in inverted PSCs with the structure of ITO/PEDOT:PSS/MAPbI$_3$(Cl)/C$_{60}$/2,9-dimethyl-4,7-diphenyl-1,10-phenanthroline(BCP)/Ag. The inverted PSCs, whose perovskite film was prepared by 1 M perovskite precursor with a thickness of ~260 nm, exhibit better comprehensive performance for saving perovskite material and reaching a relatively high *PCE* of 15.5% at the same time. Additionally, the thickness of the C$_{60}$ ETL behind the relatively thin perovskite film is further optimized to be 20 nm by comparing the simulated absorptivity of perovskite, electrical performance and impedance results with different thicknesses of C$_{60}$ ETL. Furthermore, the optimized device shows relatively high storage stability whose *PCE* maintains more than 90% of its initial efficiency after 28 days without being encapsulated in the glove box. Taking all of this into account, our results provide a simple and cost-effective method for commercializing perovskite solar cells.

## 2. Experiments

### 2.1. Materials

Chemicals purchased from Advanced Election Technology Co., Ltd. in shenyang city, Liaoning province of China: methylammonium iodide (CH$_3$NH$_3$I, >99.99%), lead (II) iodide (PbI$_2$, >99.99%), lead (II) chloride (PbCl$_2$, >99.99%), PEDOT:PSS (1.3–1.7% in H$_2$O dispersion). C$_{60}$, BCP(>99%) and Ag were purchased from Xi'an Polymer Light Technology Corp (Xi'an, China). The solvents, including *N,N*-dimethylformide (DMF), chlorobenzene (CB) and dimethyl sulfoxide (DMSO), were brought from Sigma-Aldrich in Shanghai of China. PEDOT:PSS was mixed with deionized water (vol. ratio = 1:5). All the above materials were used as received without any further purification.

### 2.2. Sample Preparation

The origin perovskite precursor used in this work was prepared according to our previous report by dissolving 1.4 M CH$_3$NH$_3$I, 1.26 M PbI$_2$, 0.14 mM PbCl$_2$ in a co-solvent of DMSO and DMF (vol. ratio = 9:1) in a glove box followed by stirring overnight at room temperature [19]. The origin precursor was then diluted as required with the above co-solvent. To prepare the sample, the ITO substrates were firstly washed by an ultrasonic

cleaning machine (KQ3200DV) with a mixture of a detergent (Decon 90) and deionized water at a volume ratio of 4% at 60 °C, and then repeatedly washed with deionized water at least three times. Subsequently, PEDOT:PSS (30 μL) mixed with deionized water was spin-coated onto the cleaned ITO substrates at 6000 rpm for 30 s in air, followed by heating on a hotplate at 120 °C for 20 min. A droplet of perovskite precursor (25 μL) with the target concentration was then spin-coated onto the pre-prepared PEDOT:PSS film at 400 rpm for 3 s and 4000 rpm for 30 s in the $N_2$-filled glove box with oxygen and moisture levels < 3 ppm. Finally, a $C_{60}$ film with different thicknesses (i.e., 20, 40 and 80 nm), a 6 nm BCP film and a 100 nm Ag electrode were deposited in sequence under high-vacuum ($5 \times 10^{-5}$ Pa) through shadow mask, resulting in an active area of 0.06 cm$^2$.
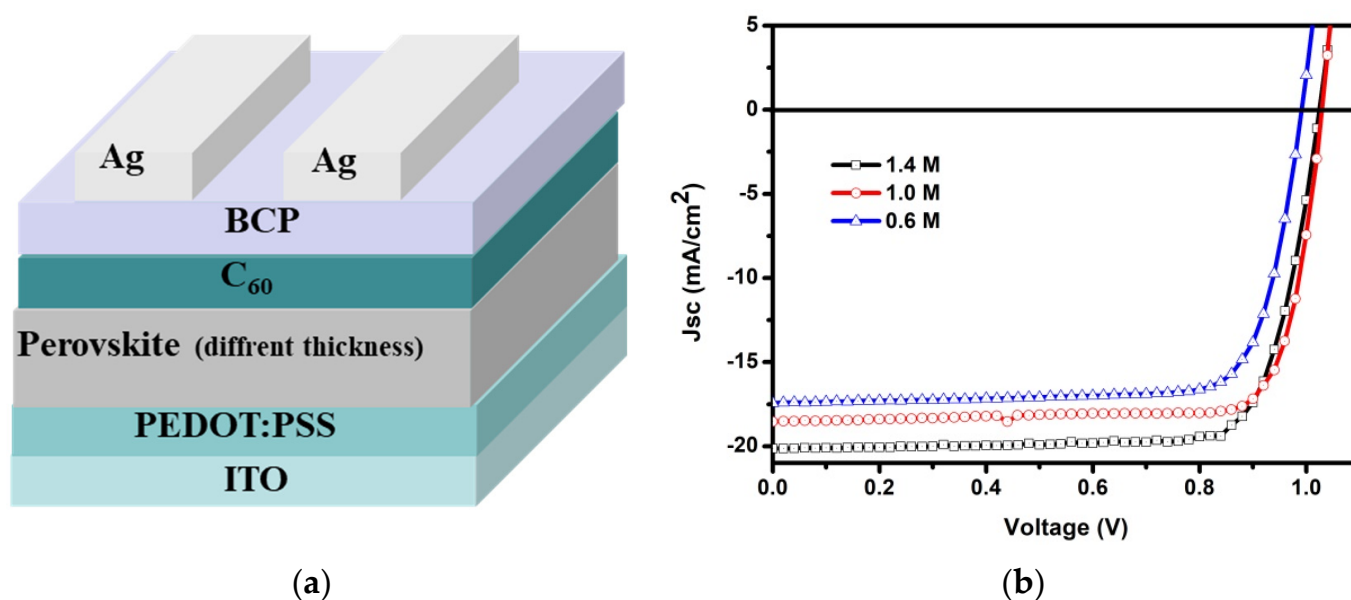
*2.3. Characterization*

The current density–voltage (*J-V*) characteristics were recorded by Keithley 2400 source meter under 100 mW/cm$^2$ simulated light (AM 1.5 G, Newport simulator: 94043A) in a glove box. During the test, the voltages were scanned from 1.2 to −0.2 V with a step of 20 mV and 0 ms delay time. The external quantum efficiency (EQE) was measured by a Newport QE system equipped with a lock-in amplifier in a glove box. The crystal and morphology characteristic of the perovskite absorption film were observed via X-ray diffraction system (Shimadzu XRD-7000) and scanning electron microscopy (SEM, JSM-6700F), respectively. The thicknesses of perovskite film prepared by different concentrations of precursor were measured by a profilometer (Kosaka ET 150). The reflection spectrum of the PSCs was carried out by UV–Visible spectrophotometer (UV-2550). The optical simulation was performed by an open source program based on the Python programming language. The detail of parameters, including refractive index, extinction coefficient and thickness of each layer, can be found in our previous work [20].

**3. Results and Discussion**

Figure 1a shows the schematic structure of an inverted PSC. As described in the introduction, our first preliminary attempt aims to obtain an inverted PSC with a better comprehensive performance, that is, achieving the balance between low material usage and relatively high PCE for commercial application. Therefore, a series of inverted PSCs, whose precursor concentrations are 1.4 M, 1.0 M and 0.6 M, respectively, were fabricated to measure and compare their electrical performance. It is worth pointing out that 1.4 M is the most commonly used precursor concentration in our group, therefore, it can be selected as reference in the following discussion. In addition, for the sake of simplicity, we will refer to *x* M device when the perovskite layer was prepared by another concentration, e.g., 1 M device represents the inverted PSCs whose perovskite film was prepared by 1 M precursor. As anticipated, the thicknesses of perovskite films gradually decrease with reducing concentrations of precursor since all precursors were spin-coated with the same coating parameters, as evidenced in Figure S1. Here, the thicknesses of perovskite films in the reference device, 1 M and 0.6 M device are~430, 265 and 190 nm, respectively.

Figure 1b displays the *J-V* characteristics of each inverted PSC prepared by different concentrations of perovskite precursors, and their corresponding photovoltaic parameters are extracted and summarized in Table 1. Clearly, decreasing the concentration of perovskite precursor leads to a decrease in device performance. Specifically, the reference device yields a *PCE* of 16.31% with a short-circuit current density ($J_{SC}$) of 20.14 mA/cm$^2$, an open-circuit voltage ($V_{OC}$) of 1.025 V and fill factor (*FF*) of 79.1%, which is in good agreement with our previous results. [2] More excitingly, the 1 M device exhibits an acceptable electrical performance with a *PCE*, $J_{SC}$, $V_{OC}$ and *FF* of 15.50%, 18.53 mA/cm$^2$, 1.03 V and 81.2%, respectively. Such laudable electrical performance indicates that the crystallinity and grain size of perovskite film prepared by 1 M precursor are not affected by decreasing its thickness, as evidenced in Figures S2 and S3, respectively. Moreover, a bit lower *PCE* is obtained in the 1 M device as compared to that of the reference device, which is mainly ascribed to the decrease in $J_{SC}$ due to the uncomplete absorption of incident light caused by

the relatively thin perovskite film. As the concentration of precursor is reduced further, the *PCE* of the 0.6 M device decreases to less than 14%, which cannot meet the requirements for commercial application. In addition, the above-mentioned change tendency was further confirmed by the external quantum efficiency (EQE) spectrum and their corresponding integral current ($J_{EQE}$). As presented in Figure S4, a dramatically decreased EQE in the wavelength range from 580–750 nm is observed in both 1 M and 0.6 M devices as compared to that of the reference device. The calculated $J_{EQE}$ of the reference device, 1 M device and 0.6 M device are 20.24 mA/cm$^2$, 18.78 mA/cm$^2$ and 18.32 mA/cm$^2$, respectively, which is in accordance with the $J_{SC}$ results extracted from *J-V* results. As shown in Figure S1, the perovskite layer decreased from 430 nm (1.4 M) to 265 nm (1.0 M), and the *PCE* decreased from 16.31% to 15.5%. That is to say, the material consumption of PSC devices is reduced by 38%, and the photoelectric conversion efficiency is reduced by only 5%. By considering the consumption of perovskite material and electrical performance from the perspective of commercial application, the 1 M device exhibits the best comprehensive performance, and our further investigations will be concentrated on this type of device.



**(a)** **(b)**

**Figure 1.** (**a**) Schematic architecture of the inverted PSCs. (**b**) *J-V* characterization of the inverted PSCs with perovskite layer prepared by different concentrations (1.4 M, 1.0 M and 0.6 M) of precursors.

**Table 1.** The photovoltaic parameters of inverted PSCs with the structure of ITO/PEDOT:PSS/perovskite (1.4 M, 1.0 M and 0.6 M)/C$_{60}$ (20nm)/BCP (6 nm)/Ag.

| Perovskite | $V_{OC}$ (V) | $J_{SC}$ (mA/cm$^2$) | FF (%) | PCE (%) |
|---|---|---|---|---|
| 1.4 M | 1.025 | 20.14 | 79.1 | 16.31 |
| 1.0 M | 1.030 | 18.53 | 81.2 | 15.50 |
| 0.6 M | 0.991 | 17.43 | 78.7 | 13.59 |

As is well known, the thickness of the perovskite absorption layer is a critical parameter for determining the absorption of incident light and then the electrical performance of PSCs. According to previously published reports, it is necessary to point out that almost all incident light can be absorbed only when the thickness of perovskite layer exceeds 450 nm [21,22]. Therefore, the incident light cannot be completely absorbed by the perovskite layer in the 1 M device because its thickness is only~265 nm (Figure S1). In other terms, a small amount of incident light can reach to the electron transport layer (ETL) behind the perovskite layer and even the Ag electrode, leading to interference between the ETL and Ag. In such instances, it is reasonable to assume that the absorption of perovskite

film in the 1 M device could be influenced by varying the thickness of the ETL, resulting in affecting its *J-V* characteristics.

Within this context, an optical simulation based on transmission matrix has been performed to get deeper insight into the influence of the thickness of the $C_{60}$ ETL on light distribution in the 1 M device. This simulation was performed by an open source program written in the Python language [23], and all calculation parameters and details can be found in our previous paper [20]. During the simulation, 1 M devices with three different thicknesses (e.g., 20, 40 and 80 nm) of $C_{60}$ ETL were selected to examine and compare. Figure 2a presents the simulated absorption of the perovskite layer in the 1 M device, which is significantly affected by tuning the thickness of the $C_{60}$ ETL. More precisely, a constant absorption in the short wavelength range (400–550 nm) is observed in the above three devices, which is attributed to the very high absorption efficiency of perovskite in this wavelength range. In contrast, a gradual but obvious red-shift of the absorption peak together with absorption fluctuation in the long wavelength range (550–800 nm) are noticed when increasing the thickness of the $C_{60}$ ETL. It should be highlighted that the long wavelength light (550–800 nm) is hardly absorbed by $C_{60}$ material [23,24], thus, the absorption fluctuation originates from the interference of the unabsorbed light between the ETL and Ag electrode. As a consequence, the total absorption of perovskite film increases when increasing the thickness of the $C_{60}$ ETL. This tendency was further confirmed by the measured absorption spectrum with the help of reflection spectrum (R(λ)) in the 1 M device (see Figure S5 in Supporting Information). Using a simple calculation, $1 - R(λ)$, one can obtain the measured absorption spectrum. As displayed in Figure 2b, a similar absorption fluctuation in the long wavelength range is observed in the 1 M device with the above three thicknesses of $C_{60}$ ETL. In sum, both the simulated and measured absorption spectrum imply that the $J_{SC}$ of the 1 M device could be further increased because of the enhancement of total absorption after optimizing the thickness of the $C_{60}$ ETL.



(a)                                                                 (b)
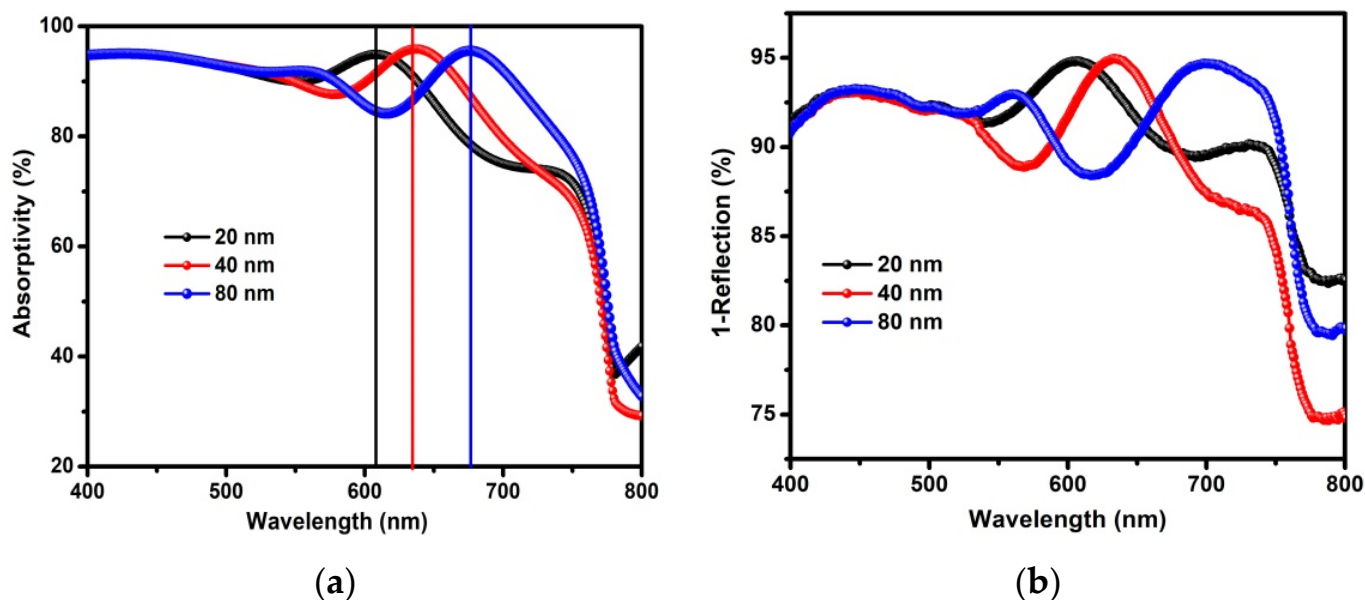
**Figure 2.** (**a**) The absorption of the 1 M device with different thickness (20 nm, 40 nm, 80 nm) of $C_{60}$ ETL calculated by optical simulation. (**b**) Measured 1-reflection spectra for the 1 M device with different thickness of $C_{60}$ ETL.

To confirm the above assumption, 1 M devices with 20 nm, 40 nm and 80 nm $C_{60}$ ETLs (hereafter named as 1 M-20 nm, 1 M-40 nm and 1 M-80 nm device, respectively) were fabricated and measured to determine the optimized thickness of the $C_{60}$ ETL. Contrary to our initial expectation, an almost constant $V_{OC}$ but a moderate decrease of the $J_{SC}$ is observed as the thickness of the $C_{60}$ ETL increases, as shown in Figure 3a. All the photovoltaic parameters are summarized in Table S1. The 1 M-40 nm device reaches a *PCE* of 15.11% with a $J_{SC}$ of 18.25 mA/cm$^2$, a $V_{OC}$ of 1.03 V, and an *FF* of 80.4%. As the thickness of the $C_{60}$ ETL increases to 80 nm, its efficiency is further decreased to 14.33%, and the $J_{SC}$ is further reduced to 17.30 mA/cm$^2$. Moreover, the gradual decrease of $J_{SC}$ was further confirmed by EQE measurements and their corresponding integral current densities (see Figure S6 in Supporting Information). It should be emphasized that the above results are confused, especially considering the increase of total absorption efficiency when increasing the thickness of the $C_{60}$ ETL.
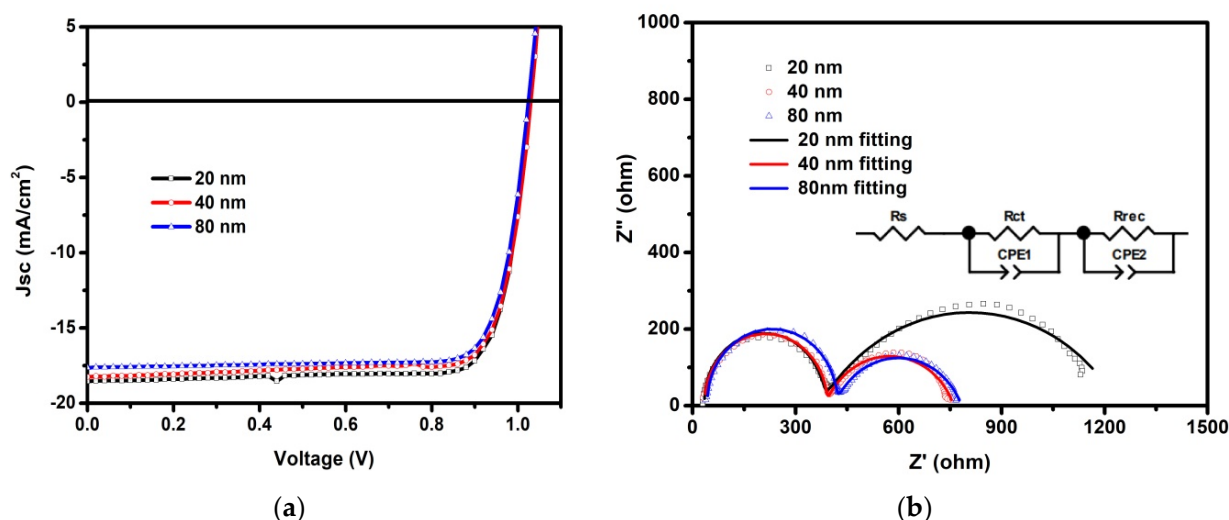


**Figure 3.** (**a**) *J-V* characterizations of the 1 M device with different thicknesses (20, 40, 80 nm) of $C_{60}$ ETL. (**b**) Nyquist plots of 1 M devices with the above different thicknesses of $C_{60}$ ETL. The inset is the equivalent circuit used for fitting.

Aiming at a better understanding of the above puzzle, the electrochemical impedance spectrum (EIS) technique was carried out to analyze the internal resistance of inverted PSCs. Figure 3b shows the Nyquist plots of 1 M devices with the three different thicknesses of $C_{60}$ ETL above, measured at a DC bias of $V_{OC}$ and under 100 mW/cm$^2$ illumination. The equivalent circuit is shown in the inset of Figure 3b, where a series resistance ($R_s$) is ascribed to resistance of the ITO and wire electrode, the transportation resistance ($R_{ct}$) is attributed to charge transfer, and the recombination resistance ($R_{rec}$) is associated with the charge recombination rate. CPE is ideal capacitors and constant phase elements [25]. Additionally, an equivalent circuit has been employed to extract values related to internal resistance, including $R_s$, $R_{ct}$ and $R_{rec}$. The fitted parameters are listed in Table S2. First of all, the resistance difference of $R_S$ is caused by the different positions of devices on ITO. Generally, the lower the $R_s$ value, the higher the FF. Thus, a better FF is obtained in the 1 M-20 nm device. In addition, $R_{ct}$ (and $R_{rec}$) values extracted from 1 M-20 nm, 1 M-40 nm, and 1 M-80 nm devices are 337 (869), 352 (373) and 372(367) $\Omega$, respectively. As is known, low $R_{tr}$ is of benefit to charge carrier transport in the active layer while high $R_{rec}$ is conducive to a reduction in charge recombination [26]. Therefore, benefiting from the lowest $R_{tr}$ and largest $R_{rec}$, the 1 M-20 nm device exhibits the highest $J_{SC}$ as well as high *PCE*, although it has a relatively low total absorption efficient of its perovskite layer among the above three devices.

Additionally, the relationship between Voc and light intensity is employed to further explore charge recombination at the different thicknesses of $C_{60}$ ETL in PSCs, as shown

in Figure S7. It is known that the slope deviates from $(kT/q)$, where k is the Boltzmann constant, T is temperature and q is the electric charge, reflecting trap-assisted recombination [27]. The PSC device based on 20 nm $C_{60}$ exhibits a slope of 1.78 $kT/q$, indicating a lower trap-assisted recombination, while the slope with 40 nm $C_{60}$ and 80 nm $C_{60}$ are 1.80 $kT/q$ and 1.88 $kT/q$, respectively. These results further confirmed that the recombination has been suppressed with the $C_{60}$ thickness decreasing, which is in agreement with the conclusion from Figure 3b.

Up to now, we have further optimized the thickness of the $C_{60}$ ETL in the 1 M device, whose structure is ITO/PEDOT:PSS/perovskite (265 nm)/$C_{60}$ (20 nm)/BCP (6 nm)/Ag (100 nm), to achieve the best comprehensive performance with a balance between electrical performance and material consumption. In regards to the stability of the 1 M-20 nm device, undoubtedly, stability is still one of biggest challenges for the commercialization of PSCs. Here, the storage stability measurement has been performed on the 1 M-20 nm device without encapsulation for more than 28 days in the glove box. For comparison, the reference device, whose perovskite film was prepared by 1.4 M precursor with 20 nm $C_{60}$ ETL, was also tested in the same manner. As shown in Figure 4a, both devices undergo a slow and gradual degradation of the *PCE* values within the test period. After 28 days continuous recording, the *PCE* of the reference device maintains more than 90% of its initial value, which is further confirmed by the normalized results (see Figure S8a). In particular, a similar *PCE* degradation behavior is noticed in the 1 M-20 nm device, suggesting the stability is not affected by decreasing the thickness of the perovskite layer covered by a 20 nm $C_{60}$ ETL. The *PCE* degradation in both devices is mainly ascribed to the reduction of $J_{SC}$ (see Figures 4b and S8b) because of almost no degradation of $V_{OC}$ and FF (see Figures 4c,d and S8c,d) within the same period. All above stability results confirm good stability performance for the 1 M-20 nm device, which is of benefit to its further commercial application.
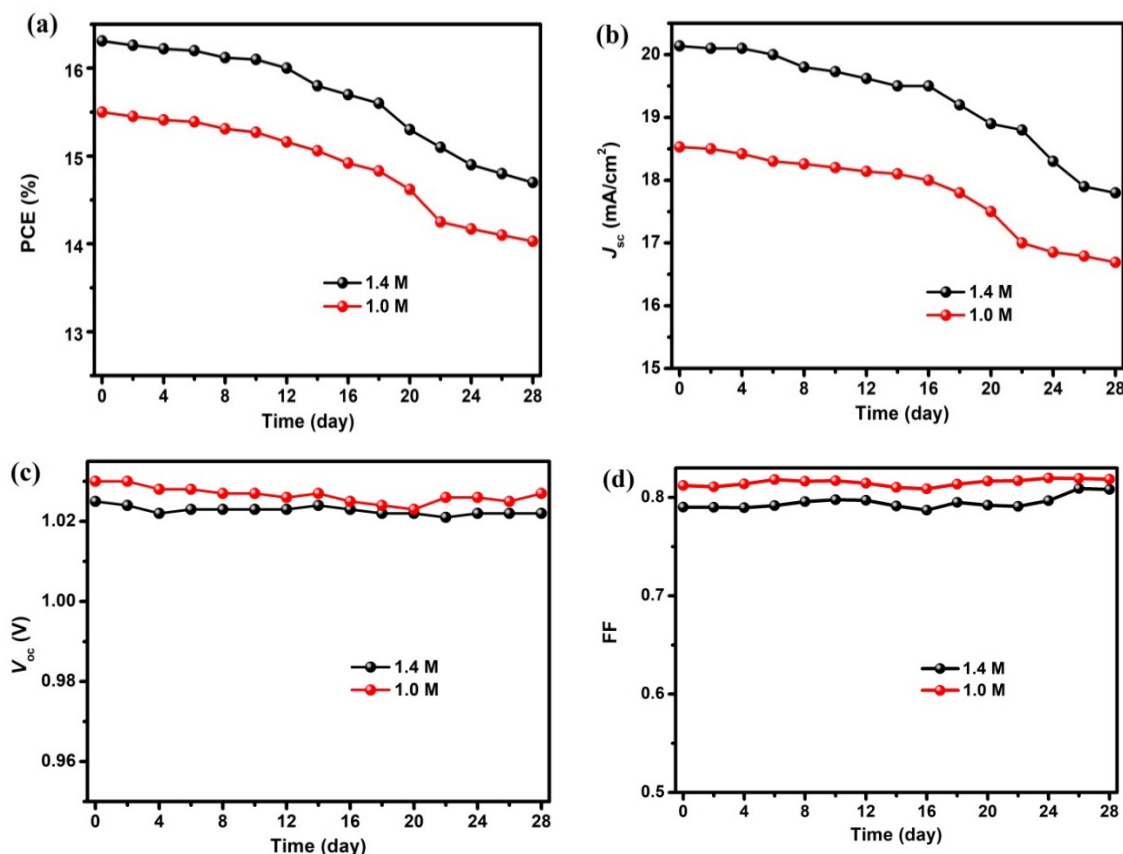


**Figure 4.** The stability of the 1 M-20 nm device and reference device stored in a glove box: (**a**) *PCE*, (**b**) *J*SC, (**c**) *V*OC and (**d**) *FF*.

## 4. Conclusions

In summary, an inverted PSC with a better comprehensive performance has been achieved by simply reducing the concentration of perovskite precursor. The inverted PSCs, whose precursor concentration is 1.0 M, yield an acceptable *PCE* of 15.50% with 18.53 mA/cm$^2$ of $J_{SC}$, 1.03 V of $V_{OC}$ and 81.2% of *FF*, reaching a balance between material consumption and its corresponding electrical performance for commercial application. Moreover, in the above 1 M device, its ETL thickness was further optimized (~20 nm) by comparing the simulated absorption spectrum, impedance spectrum and *J-V* characteristics with three different ETL thicknesses. Furthermore, the optimized device shows good storage stability, which maintains more than 90% of its initial value after one month stored in a glove box. Therefore, this study provides a simple and cost-effective method for reducing material usage in commercializing perovskite solar cells.

**Supplementary Materials:** The following supporting information can be downloaded at: https://www.mdpi.com/article/10.3390/nano12101736/s1, Figure S1: The thicknesses of perovskite films with different concentrations (1.4 M, 1.0 M and 0.6 M) of perovskite precursor. All the perovskite films were directly coated on ITO substrates; Figure S2: XRD spectra of perovskite film prepared by 1 M precursor coated on ITO/PEDOT:PSS film; Figure S3: SEM image of perovskite film prepared by 1 M precursor coated on ITO/PEDOT:PSS substrate; Figure S4: EQE spectra and their corresponding integrated photocurrents (dashed lines) of inverted PSCs with different concentration (1.4 M, 1.0 M and 0.6 M) of perovskite precursors; Figure S5: Reflection spectra of 1 M devices with different thicknesses of $C_{60}$ ETL; Figure S6: EQE spectra and their corresponding integrated photocurrents (dashed lines) of 1 M devices with different thickness (20 nm, 40 nm, 80 nm) of $C_{60}$ ETL; Figure S7: $V_{OC}$ vs. light intensity for the PSCs with different thicknesses (a) 20 nm, (b) 40 nm and (c) 80nm of C60 ETL. Figure S8: The normalized stability results displayed in Figure 4: (a) PCE, (b) $J_{SC}$, (c) $V_{OC}$ and (d) FF; Table S1: The photovoltaic parameters of 1 M devices with three different thicknesses of $C_{60}$ ETL; Table S2: Parameters of equivalent circuit extracted from the fitting of impedance data for ITO/PEDOT:PSS/Perovskite/$C_{60}$/BCP/Ag devices with different thicknesses of C60 (20, 40, 80 nm) under the illumination of AM 1.5G, 100 mW/cm$^2$.

**Author Contributions:** L.C. participated in device fabrication and wrote the paper; C.X. conceived and designed the research; Y.Q. and L.N. participated in data interpretation; X.H., H.B. and G.X. participated in data analysis; Q.S. supervised the project. All authors have read and agreed to the published version of the manuscript.

**Institutional Review Board Statement:** Not applicable.

**Informed Consent Statement:** Not applicable.

**Data Availability Statement:** The data presented in this article is available on request from the corresponding author.

**Conflicts of Interest:** The authors declare no conflict of interest.

## References

1. Ye, S.; Rao, H.; Zhao, Z.; Zhang, L.; Bao, H.; Sun, W.; Li, Y.; Gu, F.; Wang, J.; Liu, Z.; et al. A Breakthrough Efficiency of 19.9% Obtained in inverted perovskite solar cells by using an efficient trap state passivator Cu(thiourea)I. *J. Am. Chem. Soc.* **2017**, *139*, 7504–7512. [CrossRef] [PubMed]
2. Chen, L.; Xu, C.; Hu, W.; Yao, Y.; Niu, L.; Xu, G.; Zhong, Y.; Guo, P.; Song, Q. Improving the electrical performance of inverted perovskite solar cell with LiF anode buffer layer. *Org. Electron.* **2022**, *101*, 206401. [CrossRef]
3. Hu, W.; Xu, C.Y.; Niu, L.B.; Elseman, A.M.; Wang, G.; Liu, B.; Yao, Y.Q.; Liao, L.P.; Zhou, G.D.; Song, Q.L. High open-circuit voltage of 1.134 V for iInverted planar perovskite solar cells with sodium citrate-doped PEDOT:PSS as a hole transport layer. *ACS Appl. Mater. Interfaces* **2019**, *11*, 22021–22027. [CrossRef] [PubMed]
4. Chen, L.; Wang, G.; Niu, L.; Yao, Y.; Guan, Y.; Cui, Y.; Song, Q. High performance planar p-i-n perovskite solar cells based on a thin Alq$_3$ cathode buffer layer. *RSC Adv.* **2018**, *8*, 15961–15966. [CrossRef] [PubMed]
5. Best Research-Cell Efficiency Chart. 2022. Available online: https://www.nrel.gov/pv/cell-efficiency.html (accessed on 26 January 2022).

6.   Kim, M.J.; Lu, H.; Lee, T.K.; Eickemeyer, F.T.; Liu, Y.; Choi, I.W.; Choi, S.J.; Jo, Y.; Kim, H.-B.; Mo, S.-I.; et al. Conformal quantum dot-SnO$_2$ layers as electron transporters for efficient perovskite solar cells. *Science* **2022**, *375*, 302–306. [CrossRef] [PubMed]

7.   Li, X.; Zhang, W.; Guo, X.; Lu, C.; Wei, J.; Fang, J. Constructing heterojunctions by surface sulfidation for efficient inverted perovskite solar cells. *Science* **2022**, *375*, 434–437. [CrossRef]

8.   Boonmongkolras, P.; Naqvi, S.D.H.; Kim, D.; Pae, S.R.; Kim, M.K.; Ahn, S.; Shin, B. Universal passivation strategy for the hole transport layer/perovskiteinterface via an alkali treatment for high-efficiency perovskite solar cells. *Sol. RRL* **2021**, *5*, 2000793. [CrossRef]

9.   Chen, T.; He, R.; Zhang, F.; Hao, X.; Xuan, Z.; Wang, Y.; Wang, W.; Zhao, D.; Zhang, J.; Wu, L. GABr post-treatment for high-performance MAPbI$_3$ solar cells on rigid glass and flexible substrate. *Nanomaterials* **2021**, *11*, 750. [CrossRef]

10.  Lee, J.; Kim, J.; Kim, C.S.; Jo, S. Compact SnO$_2$/mesoporous TiO$_2$ bilayer electron transport layer for perovskite solar cells fabricated at low process temperature. *Nanomaterials* **2022**, *12*, 718. [CrossRef]

11.  Xu, C.; Yao, Y.; Wang, G.; Dong, J.; Xu, G.; Zhong, Y.; Lu, D.; Zhao, X.; Liu, D.; Zhou, G.; et al. Self-woven monolayer polyionic mesh to achieve highly efficient and stable inverted perovskite solar cells. *Chem. Eng. J.* **2022**, *428*, 132074. [CrossRef]

12.  Sadegh, F.; Akin, S.; Moghadam, M.; Keshavarzi, R.; Mirkhani, V.; Ruiz-Preciado, M.A.; Akman, E.; Zhang, H.; Amini, M.; Tangestaninejad, S.; et al. Copolymer-templated Nickel Oxide forhigh-efficiency mesoscopic perovskite solar cells in inverted architecture. *Adv. Funct. Mater.* **2021**, *31*, 2102237. [CrossRef]

13.  Huang, L.; Xu, J.; Sun, X.; Du, Y.; Cai, H.; Ni, J.; Li, J.; Hu, Z.; Zhang, J. Toward revealing the critical role of perovskite coverage in highly efficient electron-transport layer-free perovskite solar cells: An energy band and equivalent circuit model perspective. *ACS Appl. Mater. Interfaces* **2016**, *8*, 9811–9820. [CrossRef] [PubMed]

14.  Du, T.; Xu, W.; Xu, S.; Ratnasingham, S.R.; Lin, C.T.; Kim, J.; Briscoe, J.; McLachlan, M.A.; Durrant, J.R. Light-intensity and thickness dependent efficiency of planar perovskite solar cells: Charge recombinationversusextraction. *J. Mater. Chem. C* **2020**, *8*, 12648–12655. [CrossRef]

15.  Montoya De Los Santos, I.; Cortina-Marrero, H.J.; Ruíz-Sánchez, M.A.; Hechavarría-Difur, L.; Sánchez-Rodríguez, F.J.; Courel, M.; Hu, H. Optimization of CH$_3$NH$_3$PbI$_3$ perovskite solar cells: A theoretical and experimental study. *Sol. Energy* **2020**, *199*, 198–205. [CrossRef]

16.  Koç, M.; Soltanpoor, W.; Bektaş, G.; Bolink, H.J.; Yerci, S. Guideline for optical optimization of planar perovskite solar cells. *Adv. Opt. Mater.* **2019**, *7*, 1900944. [CrossRef]

17.  Ball, J.M.; Stranks, S.D.; Hörantner, M.T.; Hüttner, S.; Zhang, W.; Crossland, E.J.W.; Ramirez, I.; Riede, M.; Johnston, M.B.; Friend, R.H.; et al. Optical properties and limiting photocurrent of thin-film perovskite solar cells. *Energy Environ. Sci.* **2015**, *8*, 602–609. [CrossRef]

18.  Qian, Z.; Dai, X.; Shi, P.; Yin, W.; Lou, Y.; Zou, G. Discussion about ultimate efficiency of solar cells. *Sci. Bull.* **2016**, *61*, 964–970.

19.  Yu, M.; Chen, L.; Li, G.; Xu, C.; Luo, C.; Wang, M.; Wang, G.; Yao, Y.; Liao, L.; Zhang, S.; et al. Effect of guanidinium chloride in eliminating O$_2$-electron extraction barrier on a SnO$_2$ surface to enhance the efficiency of perovskite solar cells. *RSC Adv.* **2020**, *10*, 19513–19520. [CrossRef]

20.  Xu, C.Y.; Hu, W.; Wang, G.; Niu, L.; Elseman, A.M.; Liao, L.; Yao, Y.; Xu, G.; Luo, L.; Liu, D.; et al. Coordinated optical matching of a texture interface made from demixing blended polymers for high-performance inverted perovskite solar cells. *ACS Nano* **2020**, *14*, 196–203. [CrossRef]

21.  Behrouznejad, F.; Shahbazi, S.; Taghavinia, N.; Wu, H.P.; Diau, E.W.G. A study on utilizing different metals as the back contact of CH$_3$NH$_3$PbI$_3$ perovskite solar cells. *J. Mater. Chem. A* **2016**, *4*, 13488–13498. [CrossRef]

22.  Bernal-Correa, R.; Morales-Acevedo, A. Spectral reflectance optimization for planar perovskite solar cells. *Optik* **2021**, *227*, 165937. [CrossRef]

23.  Chen, L.J.; Niu, G.X.; Niu, L.B.; Song, Q.L. Effect of net carriers at the interconnection layer in tandem organic solar cells. *Chin. Phys. B* **2022**, *31*, 038802. [CrossRef]

24.  Chen, L.J.; Song, Q.L.; Xiong, Z.H.; Huang, J.H.; He, F. Environment-friendly energy from all-carbon solar cells based on fullerene-C$_{60}$. *Sol. Energy Mater. Sol. Cells* **2011**, *95*, 1138–1140. [CrossRef]

25.  Wu, R.; Yang, J.; Xiong, J.; Liu, P.; Zhou, C.; Huang, H.; Gao, Y.; Yang, B. Efficient electron-blocking layer-free planar heterojunction perovskite solar cells with a high open-circuit voltage. *Org. Electron.* **2015**, *26*, 265–272. [CrossRef]

26.  Li, S.; Li, Y.; Liu, K.; Chen, M.; Peng, W.; Yang, Y.; Li, X. Laser fabricated carbon quantum dots in anti-solvent for highly efficient carbon-based perovskite solar cells. *J. Colloid Interface Sci.* **2021**, *600*, 691–700. [CrossRef]

27.  Yang, D.; Zhou, X.; Yang, R.; Yang, Z.; Yu, W.; Wang, X.; Li, C.; Liu, S.; Chang, R.P.H. Surface optimization to eliminate hysteresis for record efficiency planar perovskite solar cells. *Energy Environ. Sci.* **2016**, *9*, 3071–3078. [CrossRef]